Protein Polarization in Isotropic Membrane Hollow-Fiber Bioreactors

D. G. Taylor
Dept. of Chemical Engineering, University of Ottawa, Ottawa, Ont., Canada K1N 6N5

J. M. Piret
Biotechnology Lab. and Dept. of Chemical Engineering, Univ. of British Columbia, Vancouver, BC, Canada V6T 1Z3

B. D. Bowen
Dept. of Chemical Engineering, Univ. of British Columbia, Vancouver, BC, Canada V6T 1Z4

A mathematical model has been developed to predict the coupled hydrodynamics and high-molecular-weight protein transport in mammalian-cell hollow-fiber bioreactors (HFBRs). The analysis applies to reactors with isotropic ultrafiltration membranes under startup conditions when the extracapillary space (ECS) is essentially unobstructed by cells. The model confirms the experimental finding that secondary ECS flows, engendered by the primary flow in the fiber lumens, can cause significant downstream polarization of ECS proteins at typical mammalian-cell HFBR operating conditions. It also reveals that the osmotic activity of the proteins, by curtailing transmembrane fluid fluxes, can influence strongly the outcome of the polarization process. In fact, at order-of-magnitude higher protein concentrations and/or lower recycle flow rates, the secondary flow velocities can be reduced by as much as six orders-of-magnitude throughout the ECS, thereby virtually eliminating the polarization problem. This result has important implications for improved reactor startup procedures.

Introduction

Hollow-fiber bioreactors (HFBRs) have been used extensively to immobilize mammalian cells for the production of diagnostic and therapeutic proteins. A HFBR consists of a bundle of cylindrical membranes (fibers) manifolded at both ends and sheathed in an outer cylindrical casing; a configuration which resembles a shell-and-tube heat exchanger. The cells are normally retained in the space between the fibers while medium flows through the fiber lumens to supply nutrients and to remove metabolic wastes. HFBRs thus protect the cells from excessive fluid shear while providing an *in vivo*-like environment conducive to high cell densities and high volumetric productivities (Piret and Cooney, 1990a). In ultrafiltration HFBRs, high-molecular-weight product proteins (for example, monoclonal antibodies) are retained and concentrated in the closed shell-side or extracapillary space (ECS).

Optimal design and operation of ultrafiltration HFBRs require consideration of some special features of these reactors. In particular, the axial pressure drop due to flow inside the lumens induces a secondary flow in the ECS. Fluid enters the ECS over an upstream portion of the reactor and then returns downstream to the fiber lumens creating a toroidal, circulating flow. This secondary flow can have significant implications for both the transport of nutrients and metabolites and the redistribution of cells and proteins in the ECS.

The hydrodynamics of packed-cell HFBRs is standardly modeled using the theory of Apelblat et al. (1974), which was developed for the analogous microscale fluid exchange between capillaries and tissues. In this approach, a single fiber, plus its associated lumen and ECS fluid, is assumed to be representative of a multifiber bundle. Flow in the lumen is taken to be laminar and essentially unidirectional, while the membrane and ECS are assumed to be isotropic porous media to which Darcy's law applies. By superimposing a solute mass balance on Apel-

Correspondence concerning this article should be addressed to B. D. Bowen.

blat's hydrodynamic theory, Salmon et al. (1988) demonstrated that convective fluid motion in the ECS can have a significant effect on low-molecular-weight nutrient and metabolite transport and hence on reactor performance. Heath et al. (1990) have also used this approach to develop a flow model for HFBRs whose ECS is filled with cells.

Mammalian-cell HFBRs sometimes operate with the ECS essentially empty of biocatalyst; for example, beta cells in the bioartificial pancreas grow only within the anisotropic membrane matrix or as a thin layer around the membrane (Chick et al., 1975). The ECS cell concentration is also very low during the startup phase of hybridoma bioreactor operations, that is, within the first few days after inoculation. Kelsey et al. (1990) have developed a hydrodynamic model for a HFBR with an unobstructed ECS. They consider, once again, a single representative fiber and its associated fluid, and solve the Navier-Stokes and continuity equations for the lumen and ECS coupled with radial Darcy flow in the membrane to obtain analytical expressions for radial and axial velocities, as well as pressure distributions throughout the reactor. Bruining (1989) also presented a model of convective flow in general hollow-fiber membrane devices based on a similar set of premises. However, because his analysis uses only radially-averaged momentum and continuity equations, it provides no direct information about the local velocity components in either the lumen or the ECS. Pillarella and Zydney (1990) employed the hydrodynamic model of Kelsey et al. to examine glucose and insulin transport in a bioartificial pancreas. They assumed that, because insulin (MW $\approx$ 6,000 kg/kmol) was present at relatively dilute concentrations and passed easily through the membrane, osmotic effects were negligible and hence the flow and transport equations could be uncoupled. They found that, under high lumen flow conditions, convective transport in the ECS can dramatically improve insulin response times. Heath et al. (1990) solved the unidirectional Navier-Stokes equation for flow in the ECS of a cell-free, single-fiber reactor and obtained good agreement with velocity profiles measured by nuclear magnetic resonance imaging. No attempt was made, however, to link the secondary ECS flow with the primary lumen flow which drives it.

There is also experimental evidence that secondary ECS flows influence the distributions of entrapped macromolecules and mobile cells under the essentially cell-free conditions that exist during startup. Waterland et al. (1975) uniformly sequestered β-galactosidase in the outer, porous support matrix of anisotropic hollow fibers and then operated the HFBR in a closed shell recycle mode. They found that, when the reactor was sacrificed after 100 min, the enzyme concentration at the downstream end of the fiber bundle was about 20 times higher than at the upstream end. Piret and Cooney (1990b) developed a freezing and sectioning method to measure the axial distributions of hybridoma cells and various high-molecular-weight proteins during the first month of a HFBR perfusion operation. Their measurements revealed not only a significant downstream polarization of proteins but also that cell growth was restricted to this end of the reactor. It was hypothesized that the scarcity of protein growth factors reduced cell growth in the upstream regions of the HFBR leading to lower cell numbers and reactor productivities. By periodically alternating the direction of medium flow in the lumen, more uniform distributions of proteins and cells were achieved and the antibody productivity was two- to threefold higher than in a unidirectional flow reactor.

The primary emphasis of this article is to study theoretically the influence that secondary ECS flows have on the transport and redistribution of high-molecular-weight proteins in an essentially cell-free HFBR. This work represents the first stage of a larger modeling effort aimed at developing a comprehensive HFBR simulator which can be used to investigate and optimize alternative operating strategies (for example, cycling of lumen flow, external recirculation of ECS fluid and vertical vs. horizontal orientation) for improving reactor performance. The hydrodynamic analysis is based on similar assumptions to those employed by Kelsey et al. (1990) except that the differential fluid mass balance is cast into a more convenient form and solved using lumen flow rather than lumen pressure boundary conditions. Furthermore, because high-molecular-weight proteins can exert significant osmotic pressures, particularly at polarized concentrations, the fluid momentum and continuity equations are intimately coupled to the differential protein mass balance. As a consequence, analytical solutions for the time-dependent concentration, velocity and pressure fields are no longer possible and numerical methods must be employed. Results are presented for the concentration polarization of bovine serum albumin (BSA) in single- or multifiber HFBRs with isotropic membranes. It is shown that protein polarization, especially when osmotic effects are accounted for, can have important implications for the operation and design of mammalian cell ultrafiltration HFBRs.

Model Development

The basic functional unit considered here (Figure 1) includes a cylindrical, isotropic ultrafiltration membrane of uniform thickness $r_2 - r_1$ surrounded by an annular ECS region having an outer radius r_3. In the case of multifiber reactors, the functional unit has a volume equal to the empty reactor volume divided by the total number of fibers and its outer envelope is taken to be a symmetry boundary. This approximate representation of a multifiber bundle implies that the fibers are uniformly spaced in the reactor cross section, and that there are no external factors, such as poor lumen flow distribution (Park and Chang, 1986) or buoyancy effects (Piret and Cooney, 1990), which may cause fluid exchange between neighboring units. In the case of single-fiber reactors, which are of interest because of their experimental simplicity (Salmon et al., 1988; Heath et al., 1990), the solid cylindrical surface encasing the ECS becomes a no-slip boundary. With these uniform hydrodynamic conditions imposed at $r = r_3$, the problem loses its angular dependency and becomes axisymmetric.

The recirculating medium enters the lumen at $z = 0$ and leaves the lumen, with the same flow rate, at $z = L$. The lumen flow creates an axial pressure gradient that causes a portion of the fluid to be bypassed through the closed and unobstructed ECS. The concentration of high-molecular-weight proteins in the inoculum is taken to be initially uniform. Because of the existence of secondary flow in the ECS, the proteins are convectively transported towards the downstream end of the HFBR. It is assumed that, within the time frame of the polarization process, the mass of proteins in the ECS remains constant. In other words, proteins are not significantly consumed or produced by metabolic reactions or adsorbed by the

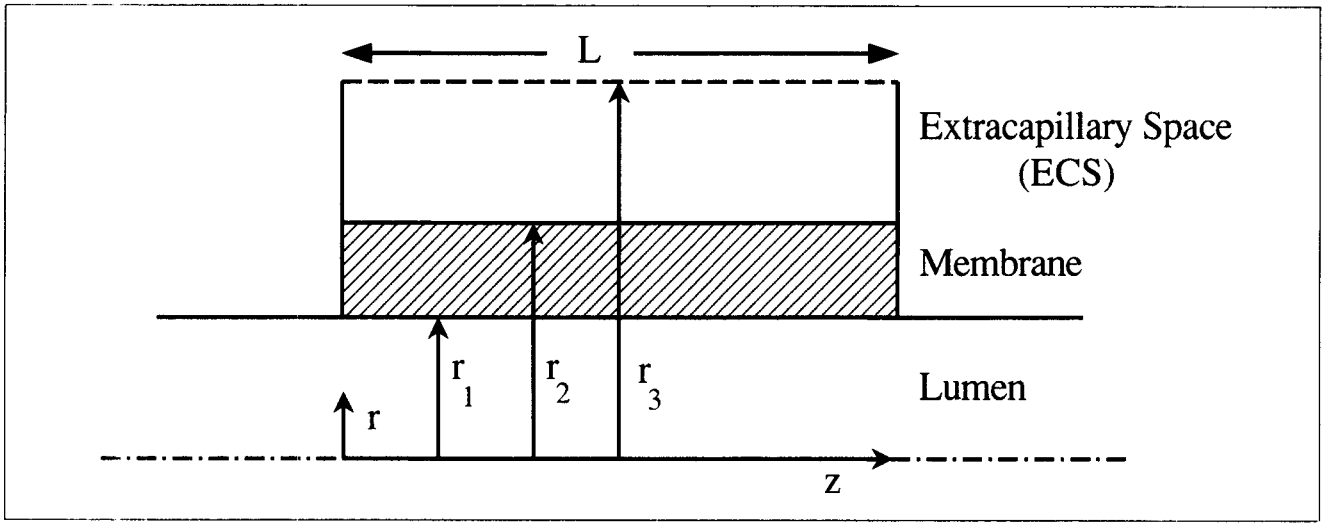

Figure 1. Basic functional unit of multi- and single-fiber HFBRs showing coordinate system and dimensions (not drawn to scale).

fibers or reactor walls. Neither do they accumulate in the isotropic membrane matrix nor escape through the membrane into the lumen. As a consequence, proteins are depleted from the upstream regions of the ECS and are polarized, often at relatively high concentrations, near the downstream end.

In the present analysis, the protein polarization process can be attenuated by two factors: diffusion and osmotic activity. Diffusion counteracts the convective transport of proteins while increased osmotic pressures in regions of protein buildup reduce the transmembrane driving force and consequently retard the local ECS flow. The concentration polarization of osmotically active solutes has been shown (Vilker et al., 1981a; Jonsson, 1984; Barious et al., 1990) to cause significantly reduced permeate fluxes in dead-end and cross-flow ultrafiltration operations. Other important mechanisms of flux retardation attributed to ultrafiltration operations, such as gel formation (Blatt et al., 1970; Trettin and Doshi, 1980) and increased hydrodynamic resistance (van den Borg and Smolders, 1989), are not considered to be significant in HFBRs. Because the transmembrane hydrostatic pressure differences are typically orders-of-magnitude lower in HFBRs, osmotic pressures are expected to control the fluid exchange between the ECS and lumen at concentrations well below the protein solubility limit.

Lumen and ECS hydrodynamics

For a constant density, constant viscosity, Newtonian fluid in the absence of body forces, the flows in the fiber lumen and ECS are governed by momentum and continuity equations having the respective general forms:

$$\frac{\partial V}{\partial t} + V \cdot \nabla V = -\frac{1}{\rho} \nabla P + \nu \nabla^2 V \tag{1}$$

and

$$\nabla \cdot V = 0. \tag{2}$$

In the above equations, V is the velocity vector, t is time, P is hydrostatic pressure and ρ and ν are the fluid density and kinematic viscosity respectively. Because the fiber is rigid and the fluid incompressible, it is assumed that the two velocity distributions adjust instantaneously to the changing osmotic pressure conditions in the ECS. Thus, only the quasi-steady form of Eq. 1 needs to be solved. Furthermore, in most HFBR applications, the flows are laminar, the membrane is relatively impermeable and the aspect ratios, r_1/L and $(r_3 - r_2)/L$, are usually less than 10^{-3}. As a consequence, radial Reynolds numbers are always small and the inertial terms of the Navier-Stokes equation can be neglected (Berman, 1953). In addition, entrance and exit effects in the lumen and end effects in the ECS can be ignored and, because axial velocity gradients are orders-of-magnitude smaller than radial gradients over most of the reactor length, the axial stress terms in Eq. 1 can be neglected.

With these simplifications, Eqs. 1 and 2 reduce to (Kelsey et al., 1990):

$$\frac{1}{r}\frac{\partial}{\partial r}\left(r\frac{\partial u}{\partial r}\right) = \frac{1}{\mu}\frac{dP}{dz} \tag{3}$$

and

$$\frac{\partial u}{\partial z} + \frac{1}{r}\frac{\partial (rv)}{\partial r} = 0 \tag{4}$$

where u and v are the axial and radial velocity components, respectively, μ is the fluid dynamic viscosity and the ordinary differential, dP/dz, in Eq. 3 implies that $P = P(z)$ only. In the lumen, Eqs. 3 and 4 are subject to the boundary conditions:

$$\frac{\partial u_L}{\partial r} = 0 \quad \text{and} \quad v_L = 0 \quad \text{at} \quad r = 0 \tag{5}$$

and

$$u_L = 0 \quad \text{at} \quad r = r_1 \tag{6}$$

while in the ECS

$$u_E = 0 \quad \text{at} \quad r = r_2 \tag{7}$$

and

$$\frac{\partial u_E}{\partial r} = 0 \quad \text{or} \quad u_E = 0 \quad \text{and} \quad v_E = 0 \quad \text{at} \quad r = r_3. \tag{8}$$

The boundary conditions expressed by Eq. 5 reflect the symmetry expected at the lumen centerline, while Eqs. 6 and 7 assume no fluid slip at the inner and outer surfaces of the membrane. The latter is only an approximation of the true fluid behavior at the junction of a free space and a permeable material (Apelblat et al., 1974). However, it is a reasonable assumption for ultrafiltration HFBRs in which axial pressure gradients are small and membrane permeabilities are very low. The first two conditions in Eq. 8 represent alternate choices between a multifiber (symmetry) or a single-fiber (no-slip) HFBR, while the last condition, which holds for both reactors, indicates that there is no fluid transfer across the external boundary of the functional unit.

The lefthand side of Eq. 3 depends only on r while the righthand side depends only on z. It is therefore integrated readily at any axial position z by treating the righthand side as a constant. When Eq. 3 is integrated twice with respect to r and the appropriate boundary conditions are applied, the following expressions for the local axial velocities are obtained:

lumen:

$$u_L = u_L(r, z) = -\frac{r_1^2}{4\mu}\frac{dP_L(z)}{dz}\left(1 - \frac{r^2}{r_1^2}\right) \tag{9}$$

ECS (multifiber):

$$u_E = u_E(r, z) = -\frac{r_2^2}{4\mu}\frac{dP_E(z)}{dz}\left[\frac{2r_3^2}{r_2^2}\ln\frac{r}{r_2} - \left(\frac{r^2}{r_2^2} - 1\right)\right] \tag{10}$$

ECS (single-fiber):

$$u_E = u_E(r, z) = -\frac{r_2^2}{4\mu}\frac{dP_E(z)}{dz}\left[\left(\frac{r_3^2}{r_2^2} - 1\right)\frac{\ln(r/r_2)}{\ln(r_3/r_2)} - \left(\frac{r^2}{r_2^2} - 1\right)\right]. \tag{11}$$

Substituting Eqs. 9, 10 and 11 in turn into 4 and integrating the result with respect to r then yields (upon application of the remaining boundary conditions) the following expressions for the local radial velocities:

lumen:

$$v_L = v_L(r, z) = \frac{r_1^3}{16\mu}\frac{d^2P_L(z)}{dz^2}\left(\frac{2r}{r_1} - \frac{r^3}{r_1^3}\right) \tag{12}$$

ECS (multifiber):

$$v_E = v_E(r, z) = \frac{1}{16\mu}\frac{d^2P_E(z)}{dz^2}\left[\frac{r_3^4}{r} - r^3 + \frac{2}{r}(r_3^2 - r_2^2)(r_2^2 - r^2) - \frac{4r_2^2}{r}\left(r_3^2\ln\frac{r_2}{r_2} - r^2\ln\frac{r}{r_2}\right)\right] \tag{13}$$

ECS (single-fiber):

$$v_E = v_E(r, z) = \frac{1}{16\mu}\frac{d^2P_E(z)}{dz^2}\left\{-\frac{r_3^4}{r} - r^3 + 2r_2^2 r + \frac{(r_3^2 - r_2^2)}{\ln(r_3/r_2)} \times \left[2r\ln\frac{r}{r_2} + \left(\frac{r_3^2 - r^2}{r}\right)\right]\right\}. \tag{14}$$

The radially-averaged lumen and ECS axial velocities, $\bar{u}_L$ and $\bar{u}_E$, respectively, are defined as

$$\bar{u}_L(z) = \frac{1}{\pi r_1^2}\int_0^{r_1} u_L(z, r)\cdot 2\pi r\, dr$$

$$\text{and} \quad \bar{u}_E(z) = \frac{1}{\pi(r_3^2 - r_2^2)}\int_{r_2}^{r_3} u_E(r, z)\cdot 2\pi r dr. \tag{15}$$

When Eqs. 9, 10 and 11 are substituted into these defining expressions, the following equations relating the axial pressure gradient and the average axial velocities in the lumen and ECS result:

lumen:

$$\frac{dP_L(z)}{dz} = -\frac{8\mu\bar{u}_L(z)}{r_1^2} \tag{16}$$

ECS (multifiber):

$$\frac{dP_E(z)}{dz} = -\frac{8\mu\bar{u}_E(z)}{\dfrac{4r_3^4\ln(r_3/r_2)}{r_3^2 - r_2^2} - 3r_3^2 + r_2^2} \tag{17}$$

ECS (single-fiber):

$$\frac{dP_E(z)}{dz} = -\frac{8\mu\bar{u}_E(z)}{r_3^2 + r_2^2 - \dfrac{(r_3^2 - r_2^2)}{\ln(r_3/r_2)}}. \tag{18}$$

Membrane hydrodynamics

Since the ultrafiltration matrix is assumed to be an isotropic, relatively impermeable porous medium, flow within the membrane is governed by Darcy's law:

$$V_M = -\frac{k}{\mu}\nabla P_M \tag{19}$$

combined with the continuity equation, Eq. 2. In Eq. 19, V_M is the membrane superficial velocity vector, P_M is the membrane pressure and k is the Darcy permeability. Because HFBR membranes have very high hydraulic resistances and very low aspect ratios, the axial pressure gradients in the lumen and ECS are typically orders-of-magnitude smaller than the radial gradients through the membrane. As a consequence, the axial component of the membrane velocity is negligible compared to the radial component. Thus, substitution of Eq. 19 into Eq. 2 yields the ordinary differential equation:

$$\frac{1}{r}\frac{d}{dr}\left(r\frac{dP_M}{dr}\right) = 0 \tag{20}$$

which is subject to the boundary conditions:

$$P_M = P_L(z) \quad \text{at} \quad r = r_1$$

and

$$P_M = P_E(z) - \Pi_E(r_2, z) \quad \text{at} \quad r = r_2 \tag{21}$$

where $\Pi_E(r_2, z)$ is the osmotic pressure exerted by the extracapillary proteins at the ECS-membrane interface. Both boundary conditions reflect the usual assumption (Apelblat et al., 1974) that the total pressure (that is, $P - \Pi$) is continuous across the interface between a porous medium and a free space while the second also requires that the proteins be completely excluded at the membrane surface (that is, the membrane reflection coefficient is unity).

When Eq. 20 is solved subject to Eq. 21 and the resulting radial pressure distribution is substituted back into Eq. 19, the following expression for the membrane superficial radial velocity, v_M, is obtained:

$$v_M = v_M(r, z) = \frac{L_p}{\mu}\frac{r_1}{r}[P_L(z) - P_E(z) + \Pi_E(r_2, z)] \tag{22}$$

where L_p ($= k/[r_1 \ln (r_2/r_1)]$) is the membrane permeability.

Overall and differential fluid balances

Once the average axial velocity is known for either the lumen or the ECS, then the corresponding radial and axial velocity components, as well as the axial pressure distribution, can be readily calculated from the equations developed above. Furthermore, since $\bar{u}_L(z)$ and $\bar{u}_E(z)$ can be related through an overall mass balance, it is only necessary to find one or the other. In the analysis which follows, an equation governing the average lumen axial velocity is obtained by carrying out a fluid mass balance over a differential length of the lumen.

Assuming that steady-state conditions prevail, the net inflow of fluid to the differential element due to the average lumen velocity must equal the net outflow due to fluid exchange between the lumen and the ECS:

$$\frac{d\bar{u}_L}{dz} = \frac{2v_M(r_1, z)}{r} = -\frac{2L_p}{\mu r_1}[P_L(z) - P_E(z) + \Pi_E(r_2, z)] \tag{23}$$

substituting for v_M *from Eq. 22. A more useful form of the above equation is obtained when both sides are differentiated with respect to* z. Substituting for the resulting axial pressure gradients by Eq. 16 and either Eq. 17 or Eq. 18 then yields:

$$\frac{d^2\bar{u}_L}{dz^2} = \frac{16L_p}{r_1^3}[\bar{u}_L - \alpha r_1^2(r_3^2 - r_2^2)\bar{u}_E] - \frac{2L_p}{\mu r_1}\frac{d\Pi_E(r_2, z)}{dz} \tag{24}$$

where

$$\alpha = [4r_3^4 \ln (r_3/r_2) - (r_3^2 - r_2^2)(3r_3^2 - r_2^2)]^{-1} \tag{25}$$

for multifiber HFBRs or

$$\alpha = \left[(r_3^2 - r_2^2)\left\{(r_3^2 + r_2^2) - \frac{(r_3^2 - r_2^2)}{\ln (r_3/r_2)}\right\}\right]^{-1} \tag{26}$$

for a single-fiber unit.

Since the total flow rate through any cross section of the system (lumen plus ECS) must be equal to the lumen flow at $z = 0$ (or $z = L$), it is easily shown that:

$$\bar{u}_E(z) = \frac{r_1^2}{r_3^2 - r_2^2}[\bar{u}_{L0} - \bar{u}_L(z)] \tag{27}$$

where $\bar{u}_{L0} \cdot \pi r_1^2$ is the lumen inlet (or exit) volumetric flow rate. When Eq. 27 is substituted into Eq. 24, the following ordinary differential equation governing the quasi-steady distribution of the average axial velocity in the lumen is obtained:

$$\frac{d^2\bar{u}_L}{dz^2} - \lambda^2\bar{u}_L = -\beta\bar{u}_{L0} - \frac{2L_p}{\mu r_1}\frac{df_{\text{osm}}[C_E(r_2, z)]}{dC_E}\frac{dC_E(r_2, z)}{dz} \tag{28}$$

where

$$\lambda = \left[\frac{16L_P}{r_1^3}(1 + \alpha r_1^4)\right]^{1/2}, \quad \beta = 16\alpha r_1 L_p, \tag{29}$$

$C_E(r_2, z)$ is the ECS protein concentration at the outer surface of the fiber, and $f_{\text{osm}}[C_E(r, z)]$ is the relationship between the protein osmotic pressure and the local protein concentration. The convection-diffusion equation governing the ECS protein distribution is discussed in the next section. Since the ECS is closed and the system is incompressible, Eq. 28 is subject to the simple Dirichlet boundary conditions:

$$\bar{u}_L = \bar{u}_{L0} \quad \text{at} \quad z = 0$$

and

$$\bar{u}_L = \bar{u}_{L0} \quad \text{at} \quad z = L. \tag{30}$$

In the absence of osmotic effects, the second term on the righthand side of Eq. 28 vanishes and analytical solutions for the lumen, membrane and ECS hydrodynamics become possible. Under these conditions, the velocity and pressure distributions have fore and aft symmetry. Thus, if the second boundary condition in Eq. 30 is replaced by the symmetry condition, $d\bar{u}_L/dz = 0$ at $z = L/2$, then Eq. 28 is easily resolved to obtain:

$$\bar{u}_L(z) = \bar{u}_{L0}\left[\left(1 - \frac{\beta}{\lambda^2}\right)\frac{\cosh[\lambda(L/2 - z)]}{\cosh(\lambda L/2)} + \frac{\beta}{\lambda^2}\right]. \tag{31}$$

An expression for the lumen pressure distribution can then be determined by conveniently assuming that $P_L = 0$ at $z = L/2$ and integrating Eq. 16 from $z = L/2$ towards $z = 0$. This procedure yields:

$$P_L(z) = \frac{8\mu\bar{u}_{L0}}{r_1^2}\left[\frac{\beta(L/2 - z)}{\lambda^2} + \left(1 - \frac{\beta}{\lambda^2}\right)\frac{\sinh[\lambda(L/2 - z)]}{\lambda\cosh(\lambda L/2)}\right]. \tag{32}$$

Thus, the absolute pressure distribution in the lumen, $P_L^a(z)$, is given by:

$$P_L^a(z) = P_{LL}^a + \Delta P_L/2 + P_L(z) \tag{33}$$

where P_{LL}^a is the absolute pressure measured at the lumen exit (at $z=L$) and ΔP_L is the total pressure drop over the length of the lumen:

$$\Delta P_L = 2P_L(0) = \frac{16\mu\bar{u}_{L0}}{r_1^2}\left[\frac{\beta L}{2\lambda^2} + \left(1+\frac{\beta}{\lambda^2}\right)\frac{\tanh(\lambda L/2)}{\lambda}\right]. \tag{34}$$

By combining Eqs. 27 and 31, an expression for the average ECS axial velocity may be obtained as:

$$\bar{u}_E(z) = \frac{r_1^2\bar{u}_{L0}}{r_3^2-r_2^2}\left(1-\frac{\beta}{\lambda^2}\right)\left[1-\frac{\cosh[\lambda(L/2-z)]}{\cosh(\lambda L/2)}\right]. \tag{35}$$

Since the ECS flow is symmetric about the axial center-plane of the reactor, there is no transmembrane fluid exchange at $z=L/2$. Thus, $P_E(L/2)=P_L(L/2)=0$, and integrating either Eq. 17 or 18 from $z=L/2$ towards $z=0$ yields:

$$P_E(z) = 8\alpha\mu r_1^2\bar{u}_{L0}\left(1-\frac{\beta}{\lambda^2}\right) \times\left[\left(\frac{L}{2}-z\right)-\frac{\sinh[\lambda(L/2-z)]}{\lambda\cosh(\lambda L/2)}\right]. \tag{36}$$

The absolute pressure in the ECS, $P_E^a(z)$, then becomes:

$$P_E^a(z) = P_{LL}^a + \Delta P_L/2 + P_E(z). \tag{37}$$

Equations 31-37 apply to both single- and multifiber HFBRs depending upon whether Eq. 25 or 26, respectively, is used to define the geometric constant α. The expressions for the multifiber reactor are equivalent to those obtained by Kelsey et al. (1990) for a closed ECS operation with specified lumen pressure boundary conditions. Analytical relationships for the lumen and ECS axial and radial velocity components, as well as the membrane radial velocity, can also be derived, if desired, from their defining equations. Note that, if the ECS protein concentration is uniform at C_{E0}, then the second term on the righthand side of Eq. 28 remains zero. Consequently, all of the analytical expressions developed in this section for symmetric fore and aft flow still apply, except that the absolute ECS hydrostatic pressure is raised everywhere by the constant osmotic pressure $\Pi_{E0}=f_{osm}(C_{E0})$ in accordance with the second condition in Eq. 21. These equations can therefore be used to initialize the ECS velocities in the transient protein redistribution process described next.

Protein transport

In the absence of volumetric sinks and sources, the time-dependent distribution of proteins within the ECS is governed by the standard convection-diffusion equation:

$$\frac{\partial C_E}{\partial t} = D\left[\frac{\partial^2 C_E}{\partial z^2}+\frac{1}{r}\frac{\partial}{\partial r}\left(r\frac{\partial C_E}{\partial r}\right)\right] - u_E\frac{\partial C_E}{\partial z} - v_E\frac{\partial C_E}{\partial r} \tag{38}$$

where $C_E=C_E(r,z)$ is the local protein concentration and D is the diffusion coefficient of the protein species. In writing this differential mass balance, it is assumed that D is independent of C_E, a reasonable approximation as long as the polarized protein concentrations do not become excessive (van den Berg and Smolders, 1989).

Equation 38 is subject to the following initial and boundary conditions:

$$\begin{aligned}
&C_E = C_{E0} && \text{at } 0\le z\le L,\ r_2\le r\le r_3,\ t=0\\
&\frac{\partial C_E}{\partial z}=0 && \text{at } z=0,\ r_2\le r\le r_3,\ t\ge 0\\
&\frac{\partial C_E}{\partial z}=0 && \text{at } z=L,\ r_2\le r\le r_3,\ t\ge 0\\
&v_E C_E - D\frac{\partial C_E}{\partial r}=0 && \text{at } 0\le z\le L,\ r=r_2,\ t\ge 0\\
&\frac{\partial C_E}{\partial r}=0 && \text{at } 0\le z\le L,\ r=r_3,\ t\ge 0.
\end{aligned} \tag{39}$$

The four boundary conditions specify that there is no net transfer of proteins across any of the four surfaces bounding the ECS. The simpler form of the second, third and fifth conditions results from the fact that the normal components of fluid velocity are zero at these surfaces (including at the hypothetical outer envelope of the functional unit representing the multifiber reactor). The fourth condition states that there is a quasi-steady balance between protein diffusion and convection at the membrane surface.

Protein properties and system parameters

Bovine serum albumin (BSA) was selected as the representative high-molecular-weight protein for the present HFBR concentration polarization study for the following reasons. First, the essential properties (diffusion coefficient, osmotic pressure behavior) are reasonably well established for BSA (for example, van den Berg and Smolders, 1989; Vilker et al., 1981b). Second, it was the protein used in many previous experimental and theoretical investigations of concentration polarization during dead-end or cross-flow ultrafiltration (for example, Shen and Probstein, 1977; Vilker et al., 1981a; van den Berg and Smolders, 1989). Finally, BSA is often the predominant protein in cell culture media.

Diffusion coefficient values for BSA have been measured and compiled from other literature sources by van den Berg and Smolders (1989) as a function of protein concentration and pH under isotonic NaCl conditions. For the range of protein concentrations of interest here (from 0 to about 100 kg/m^3) and for pH values around 7.0, they show that D varies monotonically at 25°C from approximately 6×10^{-11} to 7×10^{-11} m^2/s. At the mammalian cell culture temperature of 37°C, we assume that D is independent of protein concentration and has a constant value of about 1×10^{-10} m^2/s. Our numerical solutions demonstrate that, because the diffusivities of high-molecular-weight proteins are fairly low, axial transport in the ECS is normally dominated by convection and the precise value of D has little influence on the protein redistribution process.

Vilker et al. (1981b) have made extensive measurements of

Table 1. Parameter Values Used in Figures 2–10 Except Where Otherwise Indicated

Parameter	Symbol	Value
Lumen radius	r_1	110 μm
Membrane radius	r_2	190 μm
ECS radius	r_3	270 μm
Reactor length	L	0.20 m
Membrane permeability	L_p	1.25×10^{-13} m
Inlet lumen velocity	$\bar{u}_{L0}$	0.05 m/s
Fluid viscosity	μ	0.000695 Pa·s
Initial ECS concentration	C_{E0}	10 kg/m^3
BSA diffusivity	D	1×10^{-10} m^2/s
BSA molecular weight	M_p	69,000 kg/kmol
Salt concentration	m_s	0.15 M
Temperature	T	310 K
BSA charge number	Z_p	−20.4

the osmotic pressure of BSA as a function of its concentration in 0.15 M NaCl solutions at pH values of 4.5, 5.4 and 7.4. Their results were well represented by the following semiempirical relationship:

$$\Pi_E = f_{\text{osm}}(C_E) = \frac{RT}{M_p}\left\{[(Z_pC_E)^2 + (2m_sM_p)^2]^{1/2} - 2m_sM_p + C_E + A_2C_E^2 + A_3C_E^3\right\} \quad (40)$$

where R is the gas law constant, T is absolute temperature, M_p is the molecular weight of BSA (Vilker et al. assumed 69,000 kg/kmol), Z_p is the protein charge number, m_s is the molar salt concentration and the virial coefficients, A_2 and A_3, vary with Z_p according to

$$A_2 = -5.625\times10^{-4} - 2.410\times10^{-4}Z_p - 3.664\times10^{-5}Z_p^2$$

and

$$A_3 = 2.950\times10^{-5} - 1.051\times10^{-6}Z_p + 1.762\times10^{-7}Z_p^2. \quad (41)$$

It is assumed here that the BSA solution has a pH of 7.4, for which $Z_p = -20.4$ (Vilker et al., 1981b).

The numerical values of constants relevant to the BSA redistribution behavior are summarized in Table 1 along with the standard hydrodynamic parameters assumed for this study. The latter constants are based on measurements we have performed (Patkar et al., 1993) on an Amicon Flo-Path 7000 reactor which contains about 5,000 ultrafiltration fibers. The Amicon polysulphone membranes are actually anisotropic with a thin inner ultrafiltration skin surrounded by a thick macroporous matrix that provides structural support. Thus, the membrane permeability reported in Table 1 is likely high for the isotropic membranes under consideration here. As a consequence, L_p was reduced through several orders-of-magnitude in the parametric study described in the Results and Discussion section. Other parameters investigated in detail were the initial protein concentration, C_{E0}, and the inlet lumen velocity, $\bar{u}_{L0}$.

Numerical solution methods

Once the system parameters and initial conditions have been specified, the protein behavior in the ECS and the fluid behavior in the entire reactor can be followed with time by solving simultaneously the transient PDE (Eq. 38) for $C_E(r, z)$ and the quasi-steady ODE (Eq. 28) for $\bar{u}_L(z)$. All other system variables, including radial and axial velocity components and axial hydrostatic, osmotic and total $(P-\Pi)$ pressure distributions, can be determined directly from C_E and $\bar{u}_L$. Because the two governing equations are linked by a nonlinear osmotic pressure relationship (Eq. 40), an analytical solution is not feasible and numerical methods must be employed.

Equation 38, with its associated initial and boundary conditions (Eq. 39), was solved using finite difference methods. The time derivative was represented implicitly by a first-order, backward difference, which allows the concentration solution to be marched forward in time from the uniform condition that exists at $t=0$. The radial and axial spatial derivatives were handled by means of the "power-law" discretization scheme proposed by Patankar (1980). Upwind differencing of some type is essential in this problem because of the extreme dominance of convection compared to diffusion as a protein transport mechanism throughout most of the ECS. The "power-law" scheme provides a smooth transition from central differences when the local Peclet number (based on the grid spacing) is zero, to pure upwind differences when the Peclet number approaches infinity. At each new time level, the two-dimensional array of nodal concentration values was solved iteratively using a line over-relaxation procedure (Patankar, 1980). The converged solution from the previous time level was used to initialize this new distribution. The tridiagonal matrices that arise during this updating procedure were solved using the Thomas algorithm (Patankar, 1980).

The second-order boundary value problem for $\bar{u}_L$ (Eq. 28) with its boundary conditions (Eq. 30) was solved using a "linear shooting" procedure (Burden et al., 1981). This method takes advantage of the fact that linear ODEs with Dirichlet boundaries can be solved directly by superposition. Integration of the resulting pair of second-order ODEs was carried out by means of a fourth-order accurate Runge-Kutta method on a grid which used double the number of nodes as the axial grid in the concentration problem. In this way, velocity components required by the "power law" scheme at the midpoints between the concentration nodes can be supplied, as well as velocity and pressure solution values corresponding to the concentration grid. Note that, because each second-order ODE must be reduced to a pair of first-order ODEs in the Runge-Kutta procedure, the axial derivatives of $\bar{u}_L$ needed to calculate v_L (Eqs. 12 and 16) and v_E (Eqs. 13 and 17 or Eqs. 14 and 18) are automatically generated. The axial gradient of protein concentration, required as part of the second nonhomogeneous term in Eq. 28, was obtained by analytically differentiating the set of cubic splines fitted to the axial concentration distribution at the ECS-membrane interface.

Because the HFBR hydrodynamics and ECS protein distributions are interdependent, the two solutions must be iterated at each new time level. First, by assuming that the velocity distribution does not change between t and $t+\Delta t$, the concentration solution is updated at the latter time. Next, using the new distribution of $d[C_E(r_2, z)]/dz$ values, the velocity solution is advanced to $t+\Delta t$. The new ECS velocity components are then substituted back into Eq. 38 to yield an improved set of nodal C_E values. The two steps are repeated

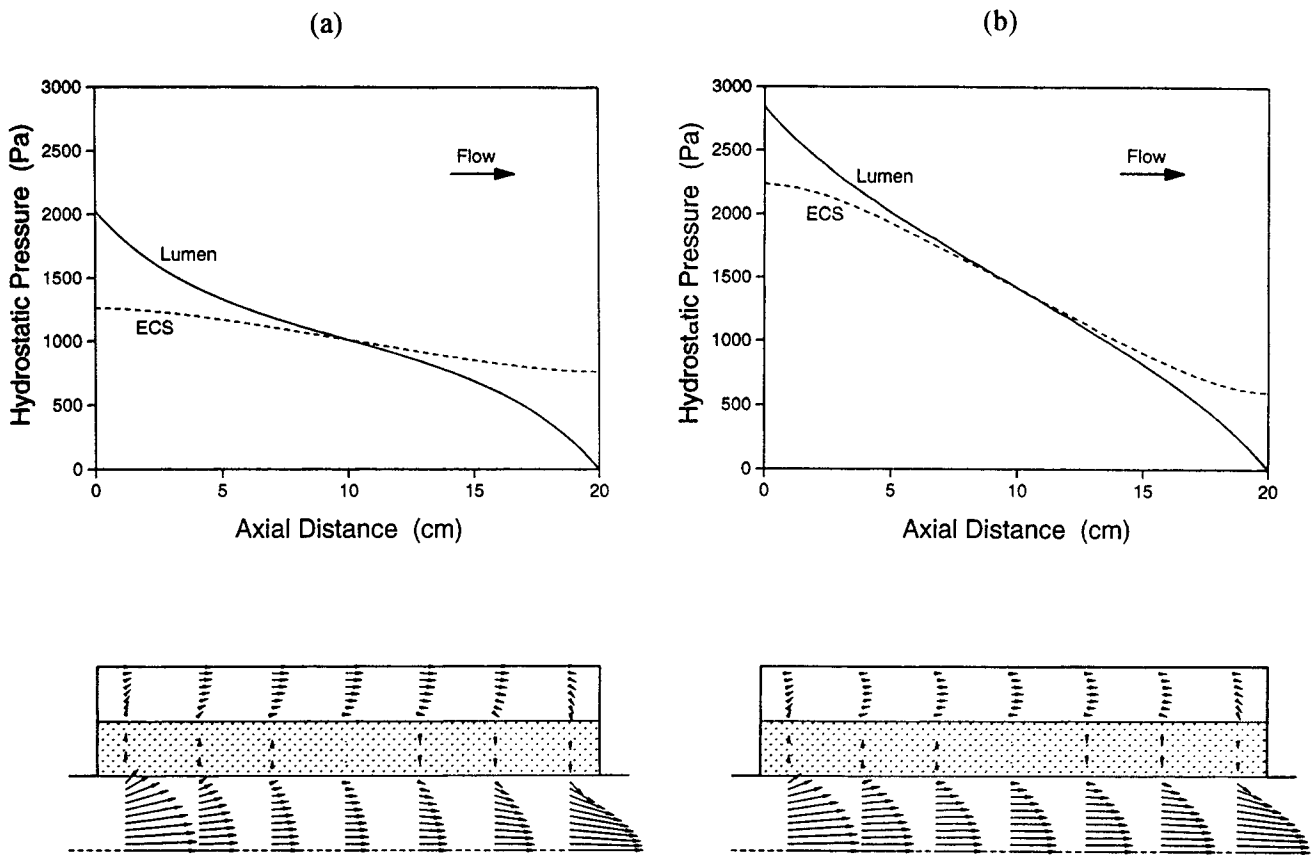

Figure 2. Hydrostatic pressure and velocity vector distributions for (a) multi- and (b) single-fiber reactors.

Parameter values as in Table 1 except $L_p = 6.25 \times 10^{-11}$ m.

until precise convergence criteria (10^{-8} kg/m^3 and 10^{-8} cm/s for C_E and $\bar{u}_L$, respectively) are met.

Only recalculation of C_E, $\bar{u}_L$, u_E and v_E is required to advance the solution over each time step. At several predetermined times, the complete solution, including lumen and ECS pressures, as well as velocity distributions in the lumen and membrane, were outputted for inspection. The integration of Eq. 16 to determine the lumen hydrostatic pressure distribution was carried out by splining the discrete values of $\bar{u}_L$ and integrating the cubic splines analytically with $P_L = P^a_{LL}$ (assumed to be 0 Pa) at $z = L$. Once $P_L(z)$ was available, the ECS hydrostatic pressure distribution was found by using Eq. 23.

The transient concentration results showed that radial concentration gradients were generally small throughout the ECS, permitting accurate solutions with fairly coarse radial grids. However, experiments with different grid sizes revealed that, unless the axial grid was sufficiently fine, "gains" or "losses" of protein occurred, especially at longer times for cases with lower initial BSA concentrations. These effects are likely a consequence of the low protein diffusion coefficient, which causes exceedingly large axial concentration gradients as steady-state is approached. All of the results reported here were obtained with an 11×501 (radial $\times$ axial) grid, for which the maximum change in protein mass never exceeded 1% even after 70,000 s of real-time simulation. Also, the initial time increments (1-10 s) were usually accelerated by a small factor (for example 1.0001-1.001) to reduce the computational effort needed to reach steady state.

Results and Discussion

Figure 2 shows the lumen and ECS hydrostatic pressure distributions, as well as the system velocity vectors for the case of a cell-free HFBR in the absence of protein osmotic effects. Hence, the analytical solution, given partially by Eqs. 31-37, applies. The hydrodynamic parameters used are those listed in Table 1 except that the membrane permeability has been increased by a factor of 500 to more dramatically illustrate the mutual dependence of the lumen and ECS flows. Also, radial dimensions, as well as radial velocity components in the vector plots, have been magnified about 200-fold for clarification. As can be seen in the upper panels, the lumen pressure exceeds that in the ECS over the upstream half of the fiber, leading to a transmembrane flux of fluid from lumen to shell. Since the ECS is closed and all the fluid entering the ECS must be returned to the lumen, the pressure and flow patterns are reversed over the downstream half. The minimum lumen flow and maximum ECS flow therefore occur at $z = L/2$ where the two pressure curves intersect. Because a fraction of the inlet fluid flow is bypassed through the ECS, the total pressure drop from the inlet to the outlet of the reactor is less than that predicted by the Hagen-Poiseuille equation for an impermeable lumen. Note that, at least in this example where the membrane permeability is artificially high, the extra ECS drag due to the no-slip boundary at $r = r_3$ in the single-fiber module causes a reduction in the ECS velocities and an increase in both the lumen and ECS pressure drops compared to the multifiber case. For the more realistic value of L_p listed in Table 1, flow

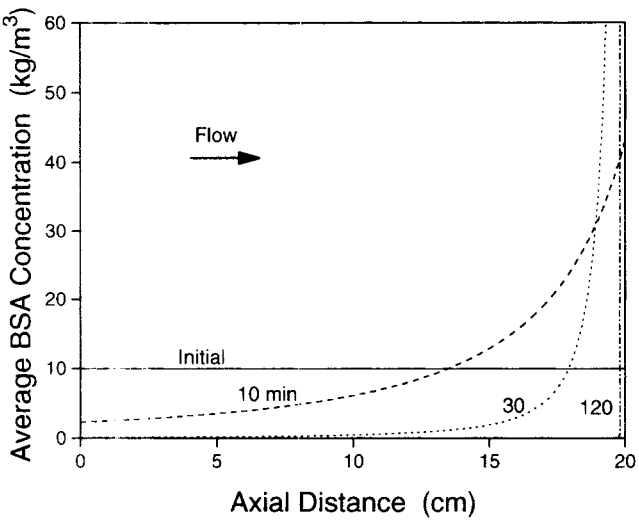

Figure 3. Radially-averaged ECS protein concentration as a function of axial distance and time for multifiber reactor with $C_{E0} = 10$ kg/m³ in the absence of osmotic effects.

in the ECS is largely governed by the membrane resistance and differences in the hydrostatic pressure distribution behavior between the two reactor types become almost indiscernible.

The flow patterns illustrated in Figure 2, which apply at $t = 0$ when the BSA solution in the ECS is homogeneous, make it visually obvious why protein polarization occurs. Figure 3 follows the variation with time of the axial distribution of radially-averaged BSA concentration for the case of a multifiber reactor where $C_{E0} = 10$ kg/m³ and where the osmotic effects of the proteins have been excluded. Under the latter circumstances, the system hydrodynamics is unlinked from the protein transport problem and, consequently, the velocity fields remain invariant with time. As can be seen in Figure 3, the proteins are swept rapidly by the secondary ECS flow towards

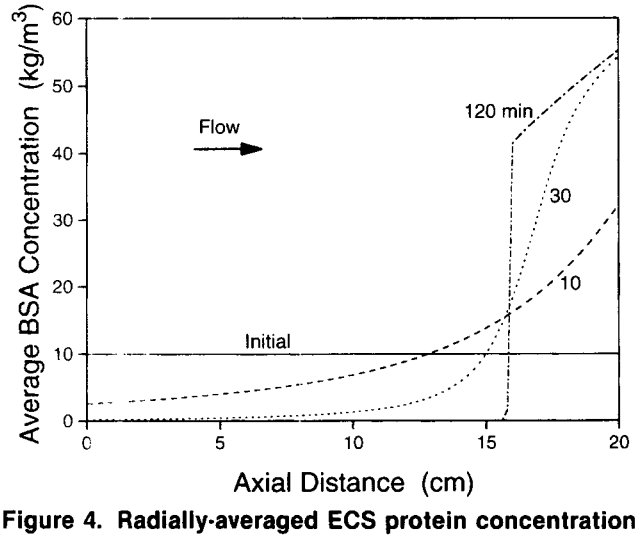

Figure 4. Radially-averaged ECS protein concentration as a function of axial distance and time for multifiber reactor with $C_{E0} = 10$ kg/m³ in the presence of osmotic effects.

the downstream end of the reactor. For this case, a numerical solution for the steady-state polarized concentration distribution is difficult to achieve. Because convective transport is dominant, diffusion does not begin to affect the concentration distribution until the proteins have been virtually eliminated from most of the ECS and have piled up in a thin layer near $z = L$. At this stage, polarization has become so extreme that the finite difference approximations begin to break down. Concentrations in this layer can exceed the solubility limit for BSA (585 kg/m³, van den Berg and Smolders, 1989).

Figure 4 demonstrates the very different BSA redistribution behavior which results for the multifiber, $C_{E0} = 10$ kg/m³ case when the osmotic pressure of the proteins, expressed by Eqs. 40 and 41, is retained in the analysis. The downstream movement of proteins starts off in a manner similar to that observed in Figure 3. However, instead of forming a thin, highly polarized layer at $z = L$ as $t \to \infty$, the BSA molecules collect in an axial region which occupies the downstream 20% of the ECS length and which has an intermediate concentration range of 41-55 kg/m³. The reason for this behavior becomes apparent when the total pressure ($P - \Pi$) distributions in the lumen and ECS are examined in Figure 5. At $t = 0$, the two total pressure curves intersect at $z = L/2$ as expected. Because the membrane permeability is at the value listed in Table 1, the transmembrane resistance is large and the ECS axial flows are much smaller than in the case of Figure 2. Consequently, the lumen pressure curve is almost linear and the ECS total pressure is relatively constant at the mean value of the lumen pressure. As the proteins are transported downstream with time, they build up, starting at $z = L$, only to the extent required for the ECS total pressure to approximately match the hydrostatic pressure on the lumen side. At this point, the transmembrane fluid flux approaches zero, producing a region of virtually stagnant fluid in the downstream portion of the ECS. Because the diffusion coefficient of BSA is so small, nearly all of the proteins become packed into this region, leaving an abrupt transition between the polarized layer and an essentially protein-free zone upstream. During this process, the crossover point between the two total pressure curves moves upstream. Thus, the regions of ECS inflow and outflow become more confined and simultaneously experience smaller transmembrane driving forces. As a consequence of these two influences, the average axial ECS velocity, plotted as a function of axial distance in Figure 6, decreases markedly with time. The maximum value of $\bar{u}_E$, which when multiplied by the cross-sectional area of the ECS yields the total inflow or outflow across the membrane, drops by about 40% from the beginning to the end of the polarization process.

Figure 7 shows the steady-state axial distributions of radially-averaged protein concentration obtained as C_{E0} is varied from 1 to 100 kg/m³ BSA for a multifiber HFBR. The corresponding lumen and ECS total pressures and average ECS velocities are plotted as functions of axial distance in Figures 8 and 9, respectively. Below a certain limiting concentration value ($C_{E0}^{crit} = 45.1$ kg/m³ for the parameters in Table 1), the system behavior demonstrates many of the same features as the 10 kg/m³ case discussed above. The BSA accumulates in a downstream region to concentrations sufficient to shut off the transmembrane flow thereby creating a protein-depleted, upstream region with diminished hydrodynamics. The downstream zone occupied by the protein solution increases as the initial con-

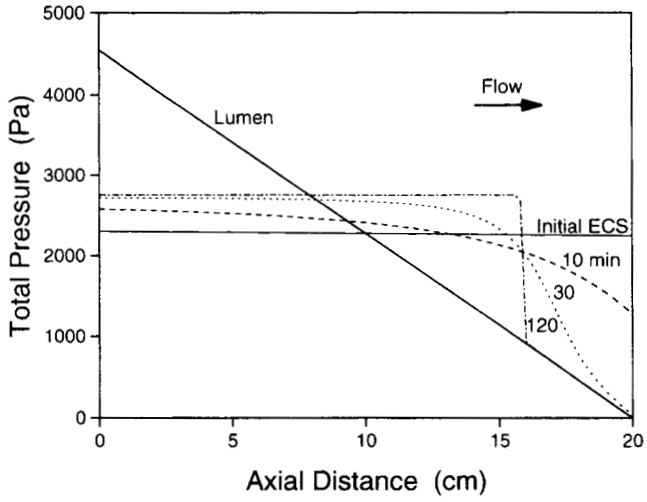

Figure 5. Lumen and ECS total pressures ($P-\Pi$) as a function of axial distance and time for multifiber reactor with $C_{E0}=10$ kg/m^3.

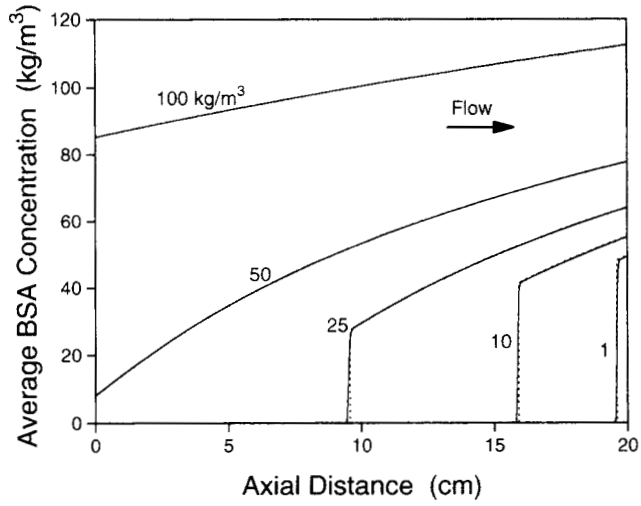

Figure 7. Steady-state distributions of radially-averaged ECS protein concentration for multifiber reactor with $C_{E0}=1$, 10, 25, 50 and 100 kg/m^3.

Solid lines—transient, two-dimensional model for $t\to\infty$; dashed lines—simple steady-state model (Appendix).

centration is raised. Above C_{E0}^{crit}, the final steady-state protein distribution fills the whole ECS and the total pressure on the shell side becomes indistinguishable from that in the lumen. Thus, the flow in the entire ECS is essentially eliminated. Of course, a very small ECS flow in the positive z-direction is still required to maintain the concentration gradient in the presence of diffusion. For example, at $C_{E0}=100$ kg/m^3, the steady-state distribution has a fairly constant axial gradient of about 140 kg/m^3·m. Thus, since axial diffusive and convective protein fluxes must be equal at steady state, it is easily calculated that $\bar{u}_E \approx 1.4\times10^{-10}$ m/s, a value which is about 6 orders-of-magnitude smaller than the average ECS axial velocities typically found in the absence of osmotic effects. It was also observed that, as the initial concentration is increased, the time taken to reach steady state at first increases, (because the ECS axial velocities are reduced) and then decreases (because the proteins need to traverse shorter distances to achieve their final distribution).

The effect of inlet lumen velocity on the steady-state radially-averaged protein distribution is shown in Figure 10 for a multifiber reactor. In all cases, the initial protein concentration was 10 kg/m^3. At very low inlet velocities, the distribution extends over the full length of the reactor, causing an almost complete stoppage in the secondary ECS flow. As $\bar{u}_{L0}$ is increased, the constant mass of proteins is packed into a downstream zone of declining length and increasing concentration. Flow in this region is essentially nonexistent while transmembrane fluid exchange is confined to the remaining upstream region which is almost protein-free. The explanation for these results is similar to that given above for the variable C_{E0} cases.

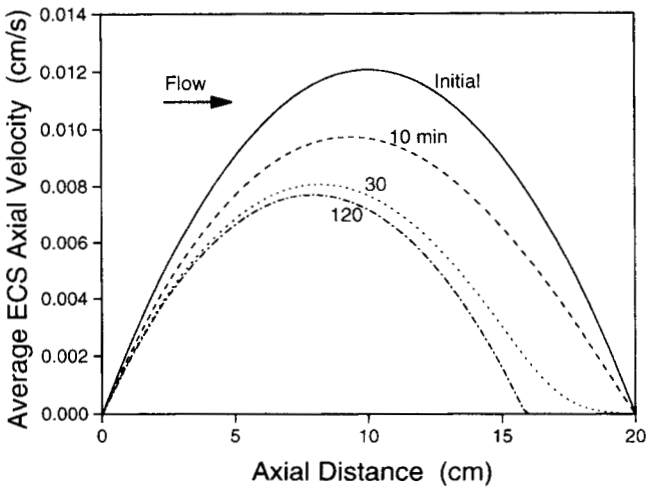

Figure 6. Radially-averaged ECS axial velocity as a function of axial distance and time for multifiber reactor with $C_{E0}=10$ kg/m^3.

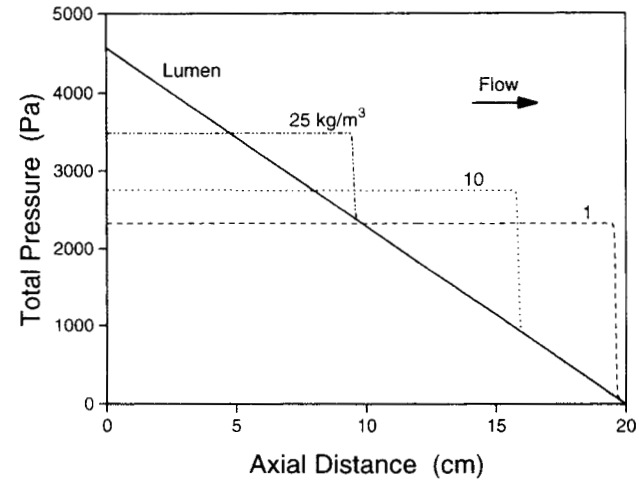

Figure 8. Steady-state distributions of lumen and ECS total pressures for multifiber reactor with $C_{E0}=1$, 10 and 25 kg/m^3.

At 50 and 100 kg/m^3, the lumen and ECS total pressures are indistinguishable.

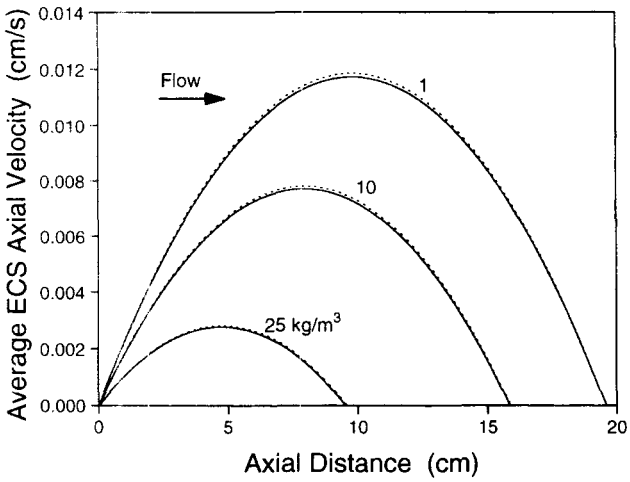

Figure 9. Steady-state distributions of radially-averaged ECS axial velocity for multifiber reactor with $C_{E0} = 1$, 10 and 25 kg/m³.

At 50 and 100 kg/m³, the average ECS axial velocities are essentially zero. Solid lines—transient, two-dimensional model for $t \to \infty$; dashed lines—simple steady-state model (Appendix).

Increasing $\bar{u}_{L0}$ engenders a larger axial pressure drop in the lumen. Thus, the proteins must accumulate to higher concentrations to produce the larger osmotic pressures needed to compensate for the steeper lumen pressure gradients. In general, the time required to reach steady state decreased as the lumen inlet velocity and hence the ECS velocities were raised.

The other system parameter that was investigated extensively was the membrane permeability. Reductions in L_p by a few orders-of-magnitude had little influence on the steady-state results, except to reduce slightly the large axial concentration gradient which exists at the boundary between the protein-rich and protein-free zones. However, they had a significant effect on the period of the transient; the time taken to reach steady state was found to be almost inversely proportional to the membrane permeability. Both the unsteady and steady-state

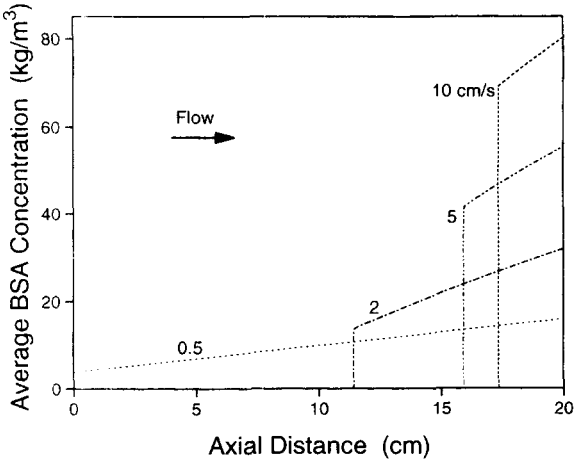

Figure 10. Steady-state distributions of radially-averaged protein concentration for multifiber reactor with $C_{E0} = 10$ kg/m³ and $\bar{u}_{L0} = 0.5$, 2.0, 5.0 and 10.0 cm/s.

trends can be explained in terms of the influence that L_p has on the ECS flow rate.

The same set of simulations was carried out for a single-fiber HFBR. The protein redistribution results bore a strong qualitative resemblance to those described above for a multifiber reactor. In fact, because the flow in the ECS is largely governed by the hydrodynamic resistance of the membrane, the final steady-state concentration, pressure and ECS average velocity distributions obtained for the single-fiber case were almost identical to the results plotted in Figures 7-10. The only noticeable differences occurred during the transients; the single-fiber results lagged slightly behind the multifiber simulations.

The above results for changes in initial protein concentration, inlet lumen velocity and membrane permeability indicate that the steady-state behavior which prevails as $t \to \infty$ may be approximated by a far simpler model. Such a model is developed in the Appendix based on the fairly gross simplifications that all of the proteins eventually accumulate in a stagnant downstream region and that flow in whatever upstream region remains is governed by a linearly falling hydrostatic pressure in the lumen and a constant hydrostatic pressure in the ECS. The results from the simple steady-state model are plotted as dashed lines on Figures 7 and 9. It is apparent that, especially as C_{E0} is raised, the simple model is able to replicate very well the steady-state results of the far more complicated transient model developed above.

Conclusions

A mathematical model has been developed to predict the hydrodynamics and protein transport in multi- and single-fiber HFBRs with isotropic ultrafiltration membranes. The model applies to the low cell density conditions of bioreactor startup and has been used to characterize the redistribution of high molecular weight ECS proteins caused by secondary ECS flows driven by axial pressure gradients in the fiber lumens. The model results qualitatively confirm previous experimental reports of β-galactosidase, antibody and transferrin polarization in the ECS of ultrafiltration HFBRs operated with unidirectional flow (Waterland et al., 1975; Piret and Cooney, 1990b).

It is shown that the polarization process can be substantially attenuated by osmotic pressures which, at higher protein concentrations, counteract the lumen/ECS hydrostatic pressure differences driving the transmembrane fluid flow. For a range of initial ECS protein concentrations and lumen inlet velocities, an abrupt transition between an upstream protein-free region and a downstream protein-polarized zone occurs as steady state is approached. The ECS flow is reduced in the upstream zone and virtually eliminated in the downstream region. At higher initial ECS concentrations or lower inlet lumen velocities, the protein distribution extends from one end of the reactor to the other, but with its gradient adjusted so that the ECS total pressure ($P - \Pi$) almost exactly balances the hydrostatic pressure variation on the lumen side. Under these conditions, the ECS flow is essentially shut down over the entire length of the reactor.

These observations suggest an alternative startup procedure for mammalian cell HFBRs which could eliminate many of the problems associated with ECS protein polarization, without the necessity of resorting to more drastic mechanical rem-

edies (for example, lumen flow cycling and ECS recirculation). Introducing a fairly concentrated solution of inert, but osmotically active, macromolecules (for example, BSA or dextrans) with the initial inocula will cause a substantial reduction in ECS flows. The consequent decreased polarization of ECS growth factors should allow more rapid cell growth over the whole length of the HFBR, leading to reduced startup times and increased bioreactor productivities. After the cell culture is well established, the initial solution of inert macromolecules can be removed from the reactor allowing restoration of the normal ECS hydrodynamics. Advantage can then be taken of the ability of the reactor to concentrate the product proteins around the downstream port of the ECS. Using a more moderate concentration of BSA and reducing the lumen flow rate should yield similar benefits during reactor startup. However, the recycle flow must remain sufficiently high to provide adequate nutrient supply to and metabolite waste removal from the immobilized cell region. In particular, oxygen depletion is a critical consideration in mammalian cell HFBRs (Heath and Belfort, 1987; Piret and Cooney, 1991).

Simulation results obtained using typical HFBR parameters reveal that flow in the ECS is largely governed by the hydrodynamic resistance of the membrane and that the axial transport of ECS proteins is mainly controlled by convective rather than diffusive effects. As a consequence, factors such as radial velocities exceeding axial velocities near the ends of the ECS and fluid viscosity as well as protein diffusivity varying with solute concentration have little influence on the polarization process. For example, the simple steady-state model developed in the Appendix, which assumes, in essence, that both the ECS fluid viscosity and protein diffusivity are zero, yielded remarkably good agreement with the predictions of the more complex transient model as $t \to \infty$. This agreement suggests that simpler transient models using, for example, radially-averaged protein concentrations and simplified hydrodynamics, may adequately represent the protein polarization behavior of most isotropic membrane HFBRs with empty shell sides.

Acknowledgment

Financial support and technical assistance for this work was provided by Amicon Canada Ltd., Amicon Division, W. R. Grace & Co. and by the Research Partners Program of the Natural Science and Engineering Research Council of Canada.

Notation

A_2, A_3 = regression coefficients in BSA osmotic pressure relationship, defined by Eq. 41
C = protein concentration, kg/m^3
D = protein diffusion coefficient, m^2/s
$f_{osm}(-)$ = osmotic pressure relationship, defined by Eq. 41 for BSA
k = Darcy's law permeability, m^2
L = reactor or fiber length, m
L_p = membrane permeability, m
m_s = molar salt concentration, kmol/m^3
M_p = protein molecular weight, kg/kmol
P = hydrostatic pressure, Pa
P^a_{LL} = absolute hydrostatic pressure at reactor exit, Pa
ΔP = hydrostatic pressure drop over reactor length, Pa
r = radial coordinate, m
r_1 = lumen radius, m
r_2 = outer membrane radius, m
r_3 = outer ECS radius, m
R = gas law constant, kJ/kmol·K
t = time, s
Δt = time increment, s
T = absolute temperature, K
u = axial velocity component, m/s
v = radial velocity component, m/s
V = velocity vector, m/s
z = axial coordinate, m
Z_p = protein charge number

Greek letters

α = geometric parameter defined by Eq. 25 or 26, m^{-4}
β = coefficient defined in Eq. 29, m^{-2}
λ = coefficient defined in Eq. 29, m^{-1}
μ = fluid dynamic viscosity, Pa·s
ν = fluid kinematic viscosity, m^2/s
Π = osmotic pressure, Pa
ρ = fluid density, kg/m^3

Subscripts

E = extracapillary space (ECS)
L = lumen
M = membrane
s = beginning of stagnant region
0 = initial condition

Superscripts

a = absolute
const = constant
crit = critical
— = radially averaged

Literature Cited

Apelblat, A., A. Katzir-Katchalsky, and A. Silberberg, "A Mathematical Analysis of Capillary-Tissue Fluid Exchange," *Biorheology*, **11**, 1 (1974).

Barious, B., S. Foyen, N. Mameri, and Y. Jarny, "Ultrafiltration in an Unstirred Cell. I. Uncharged Macromolecules at a Rejection Ratio of R = 1 in the Absence of a Gel," *Int. Chem. Eng.*, **30**, 672 (1990).

Berman, A. S., "Laminar Flow in Channels with Porous Walls," *J. Appl. Phys.*, **24**, 1232 (1953).

Blatt, W. F., A. Dravid, A. S. Michaels, and L. Nelsen, "Solute Polarization and Cake Formation in Membrane Ultrafiltration: Causes, Consequences and Control Techniques," in *Membrane Science and Technology*, J. E. Flinn, ed., Plenum Press, New York, pp. 47–97 (1970).

Bruining, W. J., "A General Description of Flows and Pressures in Hollow Fiber Membrane Modules," *Chem. Eng. Sci.*, **44**, 1441 (1989).

Burden, R. L., J. D. Faires, and A. C. Reynolds, *Numerical Analysis*, Second ed., Chapter 10, Prindle, Webber and Schmidt, Boston, MA (1981).

Chick, W. L., A. A. Like, and V. Lauris, "Beta Cell Culture on Synthetic Capillaries: An Artificial Endocrine Pancreas," *Sci.*, **187**, 847 (1975).

Heath, C. A., and G. Belfort, "Immobilization of Suspended Mammalian Cells: Analysis of Hollow Fiber and Microcapsule Bioreactors," *Adv. Biochem. Eng./Biotech.*, **34**, 1 (1987).

Heath, C. A., G. Belfort, B. E. Hammer, S. D. Mirer, and J. M. Pimbley, "Magnetic Resonance Imaging and Modeling of Flow in Hollow-Fiber Bioreactors," *AIChE J.*, **36**, 547 (1990).

Jonsson, G., "Boundary Layer Phenomena During Ultrafiltration of Dextrans and Whey Protein Solutions," *Desalination*, **51**, 61 (1984).

Kelsey, L. J., M. R. Pillarella, and A. L. Zydney, "Theoretical Analysis of Convective Flow Profiles in a Hollow-Fiber Membrane Bioreactor," *Chem. Eng. Sci.*, **45**, 3211 (1990).

Park, J. K., and H. N. Chang, "Flow Distribution in the Fiber Lumen Side of a Hollow-Fiber Module," *AIChE J.*, **32**, 1937 (1986).

Patankar, S. V., *Numerical Heat Transfer and Fluid Flow*, Hemisphere Publ. Co., New York, NY (1980).

Patkar, A., J. M. Piret, and B. D. Bowen, "Protein Adsorption in

Polysulfone Hollow Fiber Bioreactors Used for Serum-Free Mammalian Cell Culture," *Biotechnol. Bioeng.*, **42**, 1099 (1993).
Pillarella, M. R., and A. L. Zydney, "Theoretical Analysis of the Effect of Convective Flow on Solute Transport and Insulin Release in a Hollow Fiber Bioartificial Pancreas," *J. Biomech. Eng.*, **112**, 220 (1990).
Piret, J. M., and C. L. Cooney, "Immobilized Mammalian Cell Cultivation in Hollow Fiber Bioreactors," *Biotech. Adv.*, **8**, 762 (1990a).
Piret, J. M., and C. L. Cooney, "Mammalian Cell and Protein Distributions in Ultrafiltration Hollow Fiber Bioreactors," *Biotechnol. Bioeng.*, **36**, 902 (1990b).
Piret, J. M., and C. L. Cooney, "Model of Oxygen Transport Limitations in Hollow Fiber Bioreactors," *Biotechnol. Bioeng.*, **37**, 80 (1991).
Salmon, P. M., S. B. Libicki, and C. R. Robertson, "A Theoretical Investigation of Convective Transport in the Hollow-Fiber Reactor," *Chem. Eng. Comm.*, **66**, 221 (1988).
Shen, J. J. S., and R. F. Probstein, "On the Prediction of Limiting Flux in Laminar Ultrafiltration of Macromolecular Solutions," *Ind. Eng. Chem., Fundam.*, **16**, 459 (1977).
Trettin, D. R., and M. R. Doshi, "Ultrafiltration in an Unstirred Batch Cell," *Ind. Eng. Chem. Fundam.*, **19**, 189 (1980).
van den Berg, G. B., and C. A. Smolders, "The Boundary Layer Resistance Model for Unstirred Ultrafiltration, A New Approach," *J. Membrane Sci.*, **40**, 149 (1989).
Vilker, V. L., C. K. Colton, and K. A. Smith, "Concentration Polarization in Protein Ultrafiltration, Part II: Theoretical and Experimental Study of Albumin Ultrafiltered in an Unstirred Cell," *AIChE J.*, **27**, 637 (1981a).
Vilker, V. L., C. K. Colton, and K. A. Smith, "The Osmotic Pressure of Concentrated Protein Solutions: Effect of Concentration and pH of Saline Solutions of Bovine Serum Albumin," *J. Coll. Interface Sci.*, **79**, 548 (1981b).
Waterland, L. R., C. R. Robertson, and A. S. Michaels, "Enzyme Catalysis Using Asymmetric Hollow Fiber Membranes," *Chem. Eng. Comm.*, **2**, 37 (1975).

Appendix

A simple steady-state model of HFBR hydrodynamics and ECS protein redistribution is developed below. It is based on observation of Figures 4–10, which suggest the following two premises:

(1) Because typical ultrafiltration membrane permeabilities are very small, $\bar{u}_L \gg \bar{u}_E$ everywhere, and it is therefore assumed that the lumen hydrostatic pressure falls linearly with z according to the Hagen-Poiseuille equation and that the ECS hydrostatic pressure is constant.

(2) Because convective protein transfer $\gg$ diffusive protein transfer throughout most of the ECS, it is assumed that, at steady-state, all of the proteins accumulate in a downstream region of the reactor where the total ECS pressure exactly counteracts the hydrostatic pressure distribution on the lumen-side.

The implications of these two premises are as follows. Below some critical initial concentration, C_{E0}^{crit}, the ECS will divide at $z = z_s$ into two axial regions: an upstream region supporting a secondary flow and having a total (that is, hydrostatic) pressure equal to the lumen pressure at $z = z_s/2$, and a downstream region which is stagnant. Thus, since

$$P_L(z) = P_{LL}^a + \frac{8\mu\bar{u}_{L0}}{r_1^2}(L - z) \tag{A1}$$

according to Poiseuille's law, then the constant ECS pressure, P_E^{const}, will be

$$P_E^{const} = P_{LL}^a + \frac{8\mu\bar{u}_{L0}}{r_1^2}\left(L - \frac{z_s}{2}\right). \tag{A2}$$

In the stagnant region, $z_s \le z \le L$, where all of the proteins are retained,

$$\Pi_E(z) = P_E^{const} - P_L(z). \tag{A3}$$

The local protein distribution, $C_E(z)$, can now be determined from $\Pi_E(z)$, using the osmotic pressure relationships (Eqs. 40 and 41) in an implicit manner. Finally, the appropriate z_s value, required to generate this concentration distribution, must be found from a trial-and-error root-finding method by ensuring that

$$\int_{z_s}^{L} C_E(z)dz = C_{E0} \cdot L. \tag{A4}$$

Once z_s has been determined, an expression for the average axial velocity in the flow region, $0 \le z \le z_s$, can be derived from a fluid mass balance over a differential length of the ECS:

$$\frac{d\bar{u}_E}{dz} = \frac{2r_2 v_M(r_2, z)}{r_3^2 - r_2^2} = \frac{2r_1}{r_3^2 - r_2^2}\frac{L_p}{\mu}[P_L(z) - P_E^{const}]$$
$$= \frac{16L_p\bar{u}_{L0}}{r_1(r_3^2 - r_2^2)}\left[(L - z) - \left(L - \frac{z_s}{2}\right)\right] \tag{A5}$$

substituting from Eqs. A1 and A2. Integrating Eq. A5 with $\bar{u}_E = 0$ at $z = 0$ then yields:

$$\bar{u}_E(z) = \frac{8L_p\bar{u}_{L0}(z_s - z)z}{r_1(r_3^2 - r_2^2)}. \tag{A6}$$

The critical concentration corresponds to the situation where the steady-state protein distribution extends over the full length of the ECS, that is, $z_s = 0$ and, consequently,

$$P_E^{const} = P_{LL}^a + \frac{8\mu L\bar{u}_{L0}}{r_1^2} \tag{A7}$$

substituting from Eq. A2. Thus, since P_E^{const} is known from the outset, $\Pi_E(z)$ (from Eq. A3) and $C_E(z)$ can be determined and, finally, C_{E0}^{crit} can be found from

$$C_{E0}^{crit} = \frac{1}{L}\int_0^L C_E(z)dz. \tag{A8}$$

For initial concentrations greater than C_{E0}^{crit}, $C_E(z)$ extends from $z = 0$ to $z = L$ and the secondary flow is shut down over the entire length of the ECS. In this case, P_E^{const} rises above the lumen inlet pressure and must be found, using a root-finding method, by once again ensuring that Eq. A4 is satisfied. To generate the simplified steady-state results shown in Figures 7 and 9, the Newton-Raphson method was employed to invert the osmotic pressure relationship and to find either z_s or P_E^{const}, while spline quadrature was used to integrate Eqs. A4 and A8.

Manuscript received Aug. 17, 1992, and revision received June 2, 1993.